

Electronic Supplementary Information

Facet-controlled $\text{Rh}_3\text{Pb}_2\text{S}_2$ nanocage as an efficient and robust electrocatalyst toward the hydrogen evolution reaction

Taekyung Kim,^{a,b} Jongsik Park,^{a,b} Haneul Jin,^{a,b} Aram Oh,^{b,c} Hionsuck Baik,^c Sang Hoon Joo,^d
and Kwangyeol Lee^{a,b*}

^a Center for Molecular Spectroscopy and Dynamics, Institute for Basic Science (IBS), Seoul
02841, Korea

^b Department of Chemistry, Korea University, Seoul 02841, Korea

^c Korea Basic Science Institute (KBSI), Seoul 02841, Korea

^d School of Energy and Chemical Engineering, Ulsan National Institute of Science and
Technology (UNIST), Ulsan 44919, Korea

1. SYNTEHSIS AND CHARACTERISATION

Materials. Oleylamine (OAM, 98%) and lead thiocyanate ($\text{Pb}(\text{SCN})_2$, 99.5%) were purchased from Sigma-Aldrich. Rhodium acetylacetonate ($\text{Rh}(\text{acac})_3$, 97+%) was purchased from STREM chemicals. All materials were used as received.

Synthesis of PbS nanocubes. In order to prepare sharp-edged PbS nanocubes, $\text{Pb}(\text{SCN})_2$ (0.07 mmol) and $\text{Rh}(\text{acac})_3$ (0.01 mmol) were dissolved in oleylamine (5 mL) in 100 mL Schlenk tube. Subsequently, the reaction slurry was charged with Ar (1 atm) after being placed under vacuum at 100 °C for 10 min. Then the Schlenk tube containing the reaction mixtures was transferred into a 240 °C oil bath. After heating at 240 °C for 0.5 h with a magnetic stirring, the reaction mixture was cooled to room temperature, washed several times with toluene and methanol, and obtained PbS nanocubes by centrifugation.

Synthesis of $\text{PbS}@_{\text{Rh}_3\text{Pb}_2\text{S}_2}$. Rh-doped PbS nanocubes were dispersed in 1 mL toluene and mixed with $\text{Rh}(\text{acac})_3$ (0.04 mmol) in 5 mL oleylamine in 100 mL Schlenk tube. The dark brown reaction mixture was charged with 1 atm Ar after being placed under vacuum at 70 °C to remove toluene for 10 min. Then, the Schlenk tube was placed into a 220 °C oil bath, and was maintained with a magnetic stirring for another 1h. After the reaction finished, the same cooling and washing procedures as described in the PbS formation step were carried out to obtain the product.

Preparation of hollow $\text{Rh}_3\text{Pb}_2\text{S}_2$ nanocages. Core-shell structured $\text{PbS}@_{\text{Rh}_3\text{Pb}_2\text{S}_2}$ nanoparticles, redispersed in 5 mL of toluene, were etched in a solution containing 1 mL of HNO_3 and 3 mL of ethanol at 30 °C for 1h with a vigorous magnetic stirring to give hollow $\text{Rh}_3\text{Pb}_2\text{S}_2$ nanocages. After the mixture stirred for 1h, insoluble salts were allowed to settle for 10 min. The supernatant containing hollow $\text{Rh}_3\text{Pb}_2\text{S}_2$ nanocages was carefully collected by using syringe. The same washing procedures were applied to obtain the product as described in the PbS and $\text{PbS}@_{\text{Rh}_3\text{Pb}_2\text{S}_2}$ formation steps.

Preparation of $\text{Rh}_3\text{Pb}_2\text{S}_2$ nanocages with undefined facets. All procedures were the same as preparation of hollow $\text{Rh}_3\text{Pb}_2\text{S}_2$ nanocages except for not including $\text{Rh}(\text{acac})_3$ during the preparation step of PbS nanocubes.

Characterisation. The transmission electron micro-copy (TEM) and high resolution TEM (HRTEM) images were taken on a TECNAI G2 F30 ST (300 kV) and TECNAI G2 20 S-Twin (200 kV), respectively. The energy-dispersive X-ray spectroscopy (EDS) data and elemental maps in Fig. 1 were recorded with the energy dispersive X-ray spectrometer in the TECNAI G2 F30 ST. For the reaction intermediates analysis, high spatial resolution EDS study and high angle annular dark field-scanning TEM (HAADF-STEM) were performed at FEI Nanoport in Eindhoven using a Titan Probe Cs TEM 300kV with Chemi-STEM technology. EDS elemental mapping for intermediates were obtained by using a Super-X detector with XFEG. X-ray diffraction (XRD) patterns were obtained from a Rigaku Ultima III diffractometer system with a graphite-monochromatised $\text{CuK}\alpha$ radiation at 40 kV and 40 mA. X-ray photoelectron spectroscopy (XPS) was performed on a UIVAC PHI / X-Tool. The detector angle was set at 45° and the incidence

angle of X-ray was set at 90°. The amounts of metal contents in catalysts were determined by inductively coupled plasma atomic emission spectroscopy (ICP-AES) analyser (700 ES, Varian).

2. PREPARATION FOR WORKING ELECTRODE AND ELECTROCHEMICAL CHARACTERISATION

Preparation for working electrode. In order to pre-prepare ink for evaluating the electrocatalytic HER performance, 5 mg of synthesized nanoparticles, which were supported by carbon black Vulcan XC-72R powder (20 wt%), was mixed with 480 μL of ethanol (anhydrous, Sigma-Aldrich), 500 μL of D.I. water, and 20 μL of Nafion (5 wt%, Sigma-Aldrich). Subsequently, the mixture was ultrasonicated for at least 30 min with cooling. Rotating disk electrode (RDE) was polished with 1 μm size of diamond suspension and 0.05 μm size of alumina suspension. 2 μL of the ink was dropped on the polished RDE (0.071 cm^2) and spun at 800 rpm for 10 min. Thereafter, the electrode was put into a 60 °C oven for at least 5 min to be completely dried. For obtaining the XRD patterns after durability test, carbon paper (Spectracarb, 2050A-0850, FuelCellStore) electrode was used instead of RDE due to requirement for large amount of catalysts. To prepare for the electrode, ink was formulated as follows: 4 mg of synthesized nanoparticles were dispersed in aforementioned 480 μL of ethanol with 20 μL of Nafion, then the ink was ultrasonicated for 30 min with cooling. Carbon paper was ultrasonicated in acetone for 30 min and dried in 60 °C oven for at least 5 min before use. All amount of ink was dropcasted on the carbon paper (size = 2 cm x 4 cm) by syringe. To prevent ink from soaking out, careful dropping and drying were required repeatedly. Thereafter, the carbon paper electrode was put into a vacuum chamber for 6 h for complete drying.

Electrochemical characterisation. All electrochemical studies were carried out in a standard three electrode system controlled using a CHI 750E (CH Instruments) electrochemistry workstation at room temperature and humidity in 0.5 M H_2SO_4 (96%, Suprapur grade, Merck). The standard three electrode system consisted of graphite rod, Ag/AgCl (saturated KCl) electrode, and glassy carbon with 0.071 cm^2 area electrode used as counter electrode, reference electrode, and working electrode, respectively. All electrochemical data in this paper were provided as form of reversible hydrogen electrode (RHE) scale by measuring open circuit voltage of Ag/AgCl with homemade RHE ($\text{H}^+|\text{H}_2$ equilibrium on Pt electrode) to be calibrated before using every electrolyte.¹ For the purging electrolyte before electrochemical measurements to get rid of impurities, highly pure N_2 gas (99.9999%) was bubbled in the 0.5 M H_2SO_4 solution for 15 min. The electrochemical cleaning was proceeded to remove residual ligands on the surface by cyclic voltammetry (CV) in the potential range of 0.05 V - 1.1 V (vs. RHE) with a scan rate of 0.2 V sec^{-1} for 20 cycles. Electrochemical impedance spectroscopy (EIS) was conducted in a frequency range from 10 kHz to 1 Hz at -70 mV (vs. RHE) with the potential amplitude of 5 mV sec^{-1} and x-intercept of Nyquist plot at the high frequency region was selected for iR -compensation. Then, 10 CV cycles were measured to check the robustness of hydrogen evolution performance. Finally, electrochemical activity was assessed by linear sweep voltammetry (LSV) with an electrode rotation (1,600 rpm) at a scan rate of 5 mV sec^{-1} . For evaluating long-term cycling test, the continuous 5,000 and 10,000 CV cycles were measured with a sweep rate of 50 mV sec^{-1} from -

0.3 V to 0.1 V (vs. RHE) at a rotation speed of 1,600 rpm. The XRD patterns after 10,000 CV cycles were obtained by using carbon paper electrode. (See Preparation for working electrode for details.) In order to compare electrochemically active surface areas (ECSAs) between PbS@Rh₃Pb₂S₂/C and Rh₃Pb₂S₂/C catalysts, the electrochemical double-layer capacitances were measured in a non-Faradaic region at the following scan rate: 0.01, 0.02, 0.08, 0.1, 0.15, and 0.2 V sec⁻¹. The ECSAs of catalysts have relations among charging currents, scan rate, capacitance of samples according to C. C. L. McCrory et al.² by equation (1) and (2):

$$i_c = \nu C_{dl} \quad (1)$$

$$\text{ECSA} = C_{dl} / C_s \quad (2)$$

where i_c is the charging current, ν is the scan rate, C_{dl} is the double-layer capacitance, C_s is the specific capacitance of the sample. From these equations and C_s of Rh (0.025 mF cm⁻²)³, double-layer capacitance and ECSAs of PbS@Rh₃Pb₂S₂/C and Rh₃Pb₂S₂/C were calculated.

3. Supporting Fig. S1-S14 & Table S1-S2

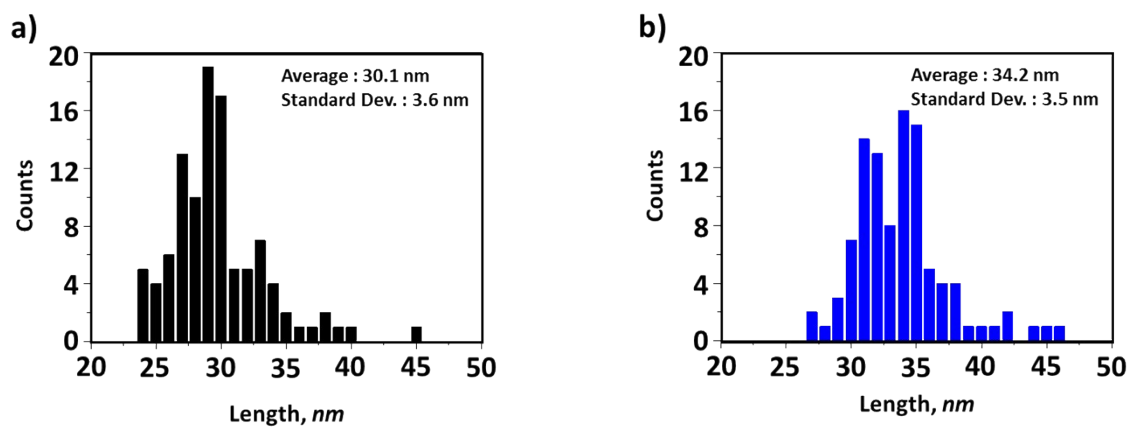


Fig. S1 The size distributions of (a) Rh-doped PbS nanocubes and (b) PbS@Rh₃Pb₂S₂ nanoparticles.

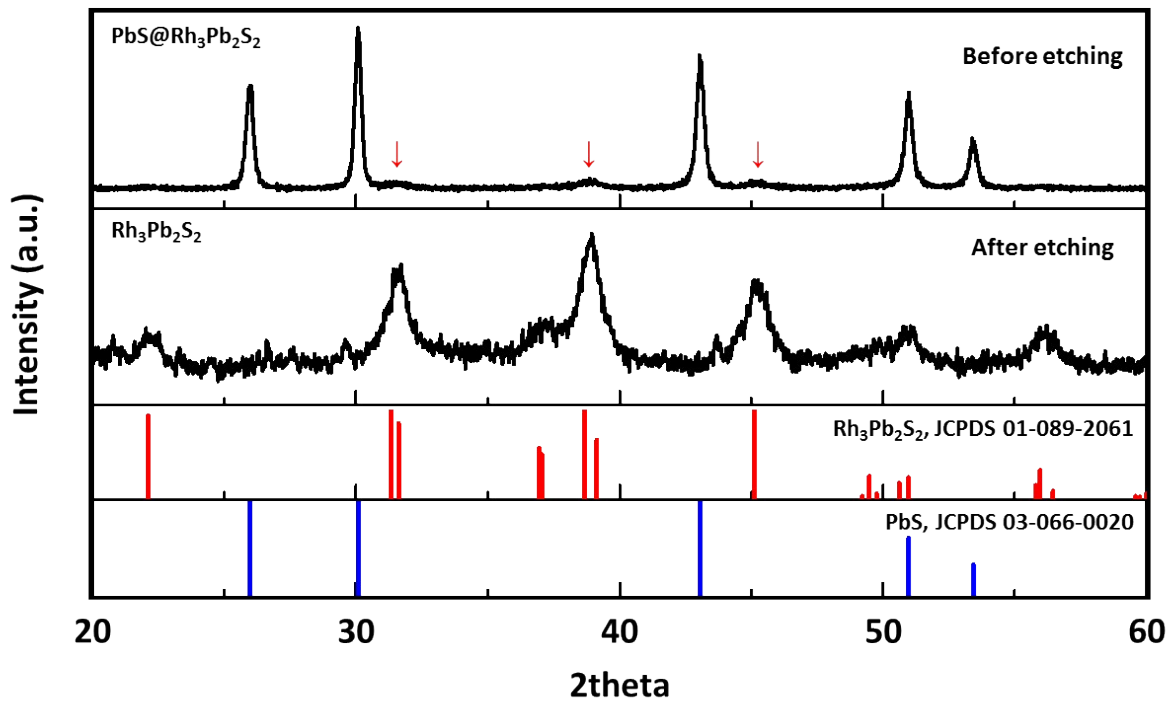


Fig. S2 Comparison of X-ray diffraction patterns (XRD): PbS@Rh₃Pb₂S₂ (before etching) and Rh₃Pb₂S₂ (after etching) are displayed.

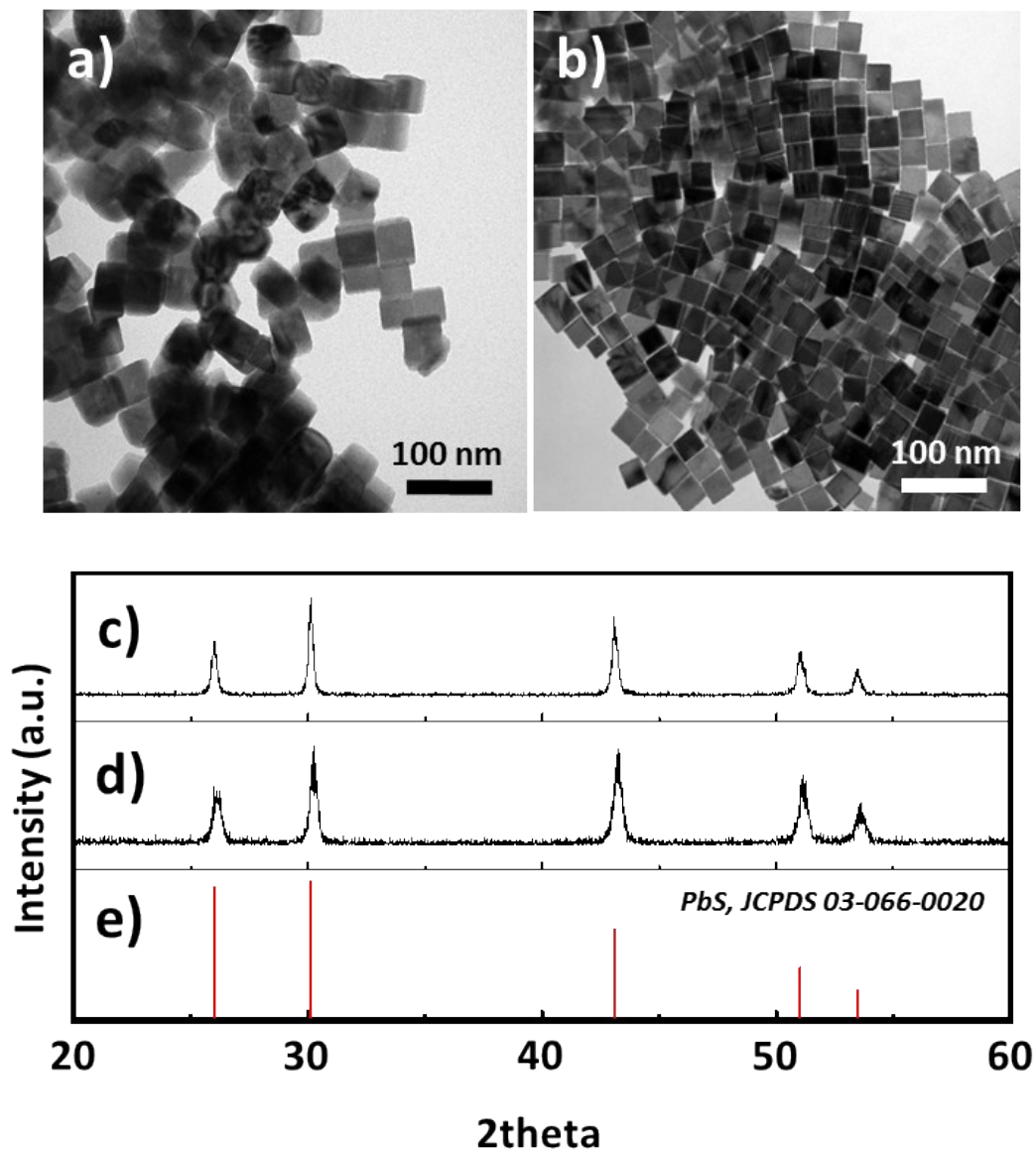


Fig. S3 TEM images of (a) PbS and (b) Rh-doped PbS nanocubes. (c), (d), and (e) are their corresponding X-ray diffraction (XRD) patterns and reference PbS data, respectively.

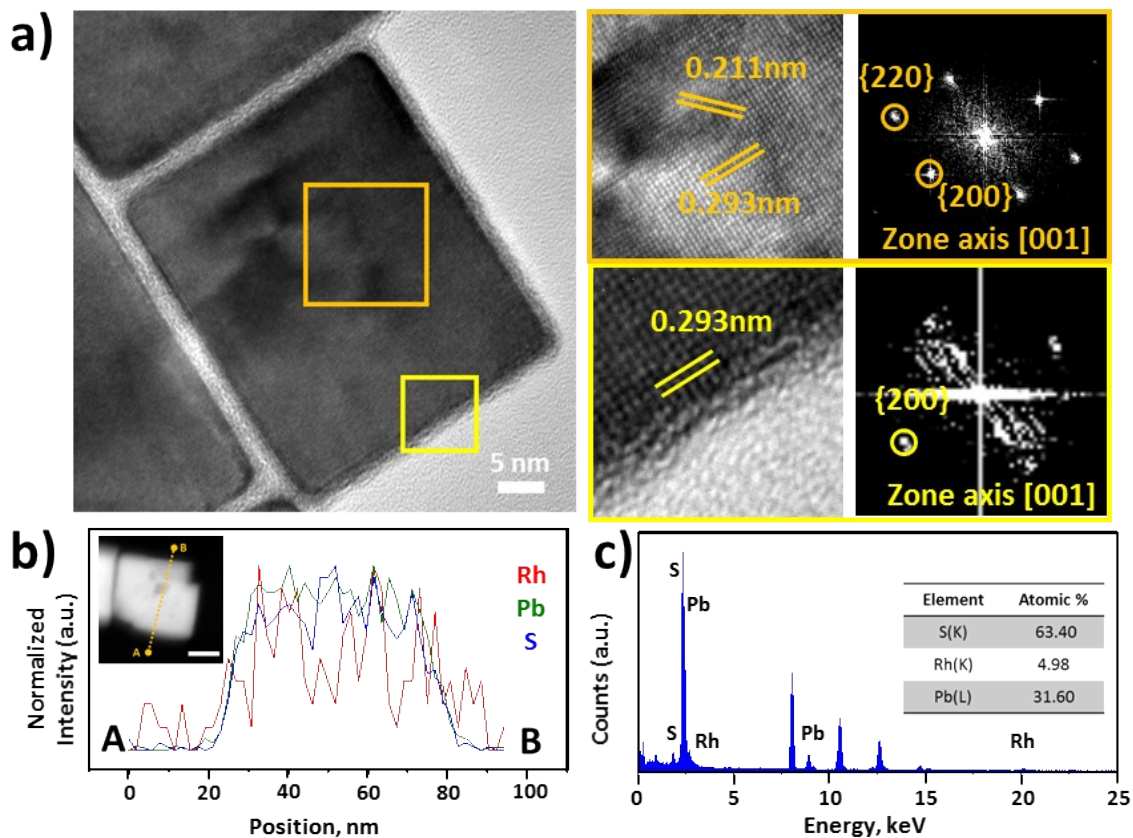


Fig. S4 The analysis results for Rh-doped PbS nanocubes: (a) fast Fourier transformation (FFT) patterns and high resolution TEM (HRTEM) images, (b) line profiles, and (c) energy dispersive X-ray spectrum (EDS). Scale bar in inset of (b) is 20 nm.

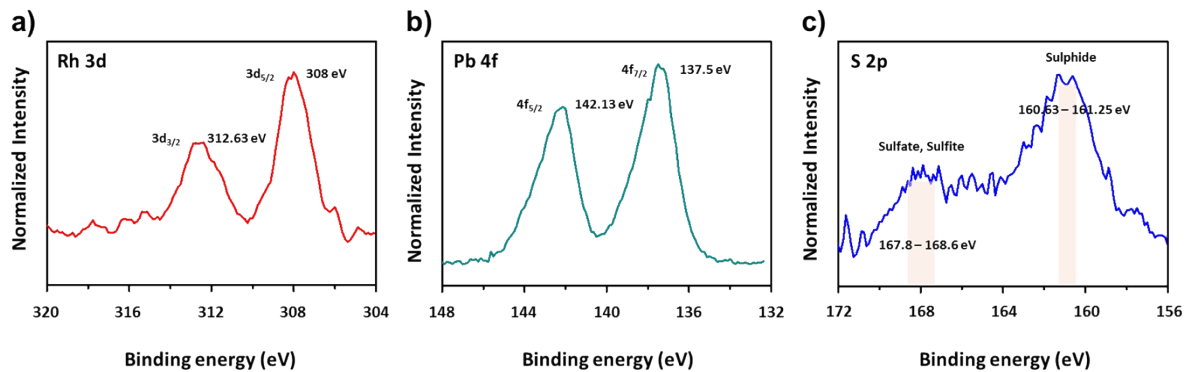


Fig. S5 X-ray photoelectron spectroscopy (XPS) spectra of Rh-doped PbS nanocubes. (a), (b), and (c) correspond to Rh 3d, Pb 4f, and S 2p peaks, respectively.

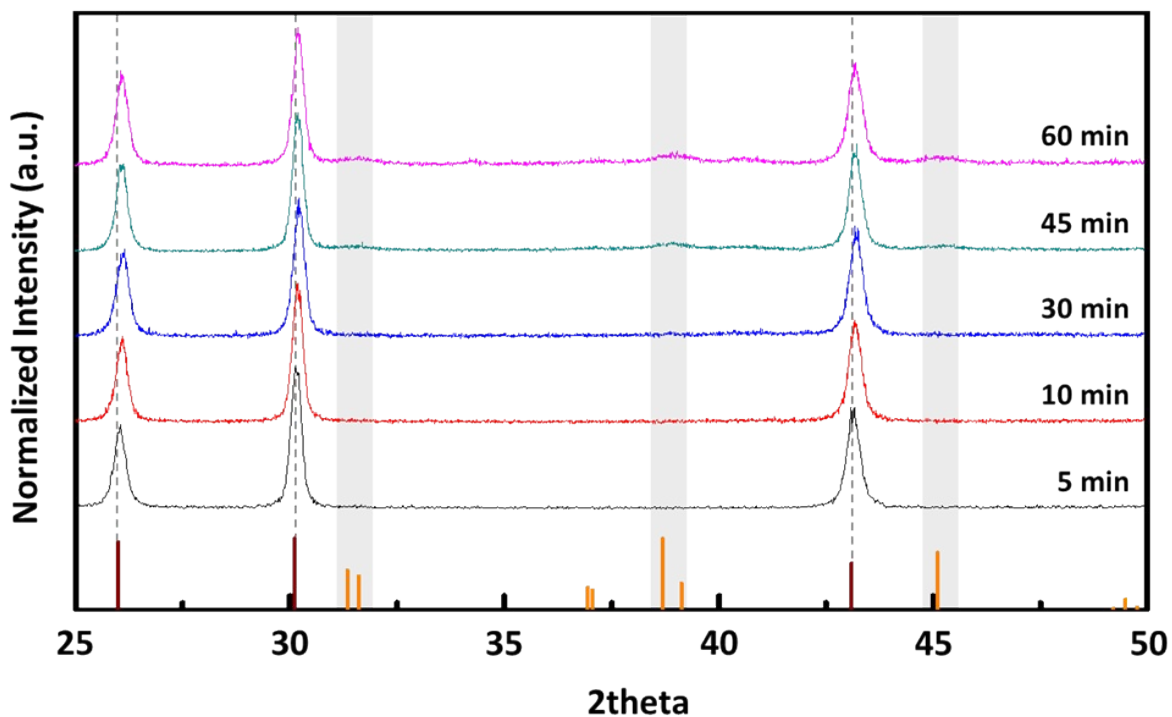


Fig. S6 Temporal XRD patterns of intermediates to $\text{PbS}@Rh_3\text{Pb}_2\text{S}_2$. JCPDS card no. 03-066-0020 for PbS (reddish brown line) and JCPDS card no. 01-089-2061 for $\text{Rh}_3\text{Pb}_2\text{S}_2$ (orange line) are displayed.

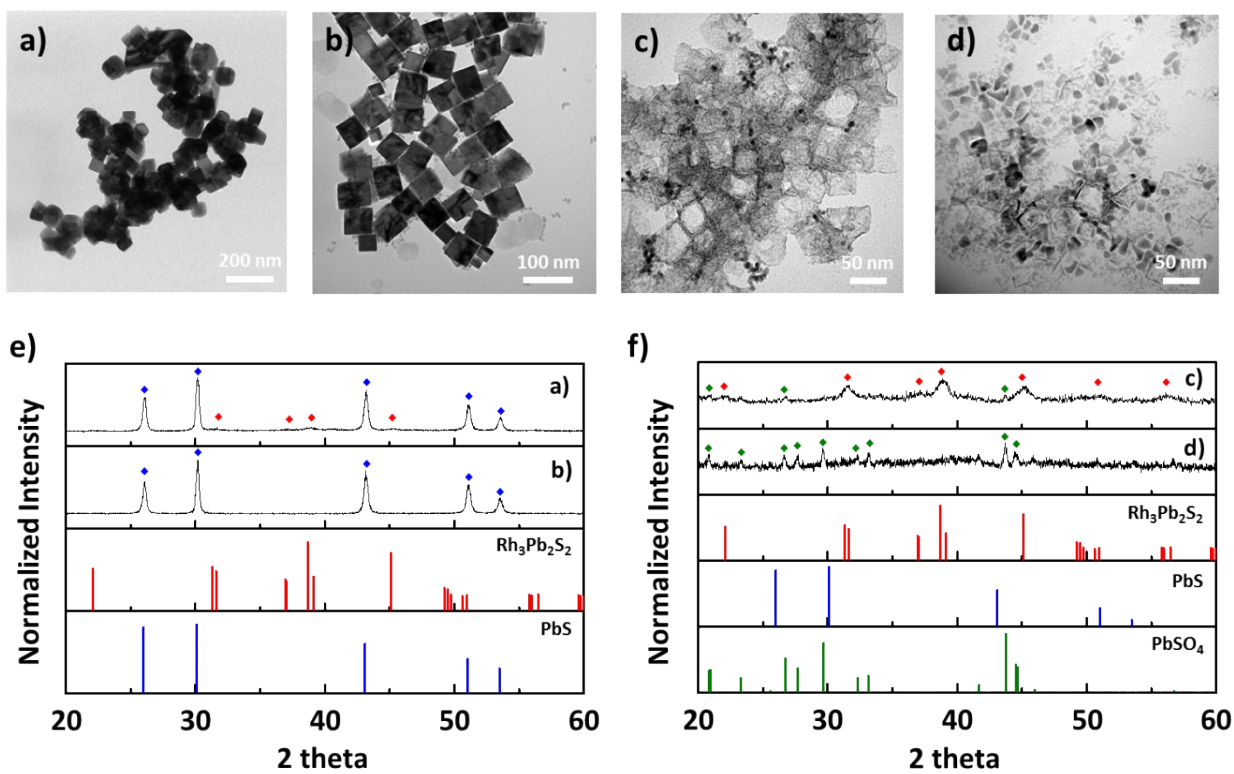
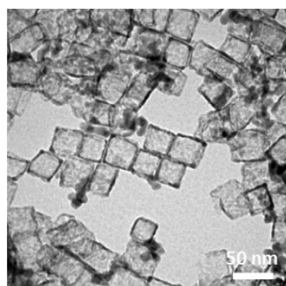
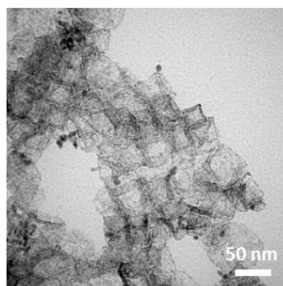


Fig. S7 TEM images of nanoparticles (a) after two-step reaction without Rh, (b) one-pot reaction, (c) and (d) are their corresponding TEM images after etching are exhibited, respectively. XRD patterns of (e) and (f) were corresponded to (a)-(b) and (c)-(d), respectively. JCPDS card no. $\text{Rh}_3\text{Pb}_2\text{S}_2$, JCPDS 01-089-2061(red), PbS, JCPDS 03-066-0020(blue), PbSO_4 , JCPDS 00-036-1461(green) are indicated.

a)

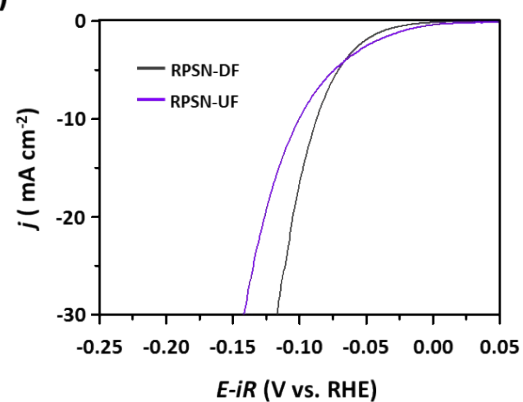


**Rh₃Pb₂S₂ nanocages
with defined facets
(RPSN-DF)**



**Rh₃Pb₂S₂ nanocages
with undefined facets
(RPSN-UF)**

b)



Overpotentials @ -10 mA cm ⁻²	
RPSN-DF	87.3 mV
RPSN-UF	100.3 mV

Fig. S8 (a) Rh₃Pb₂S₂ nanocages with defined facets(left) and undefined facets(right) and (b) their corresponding HER polarization curves are displayed.

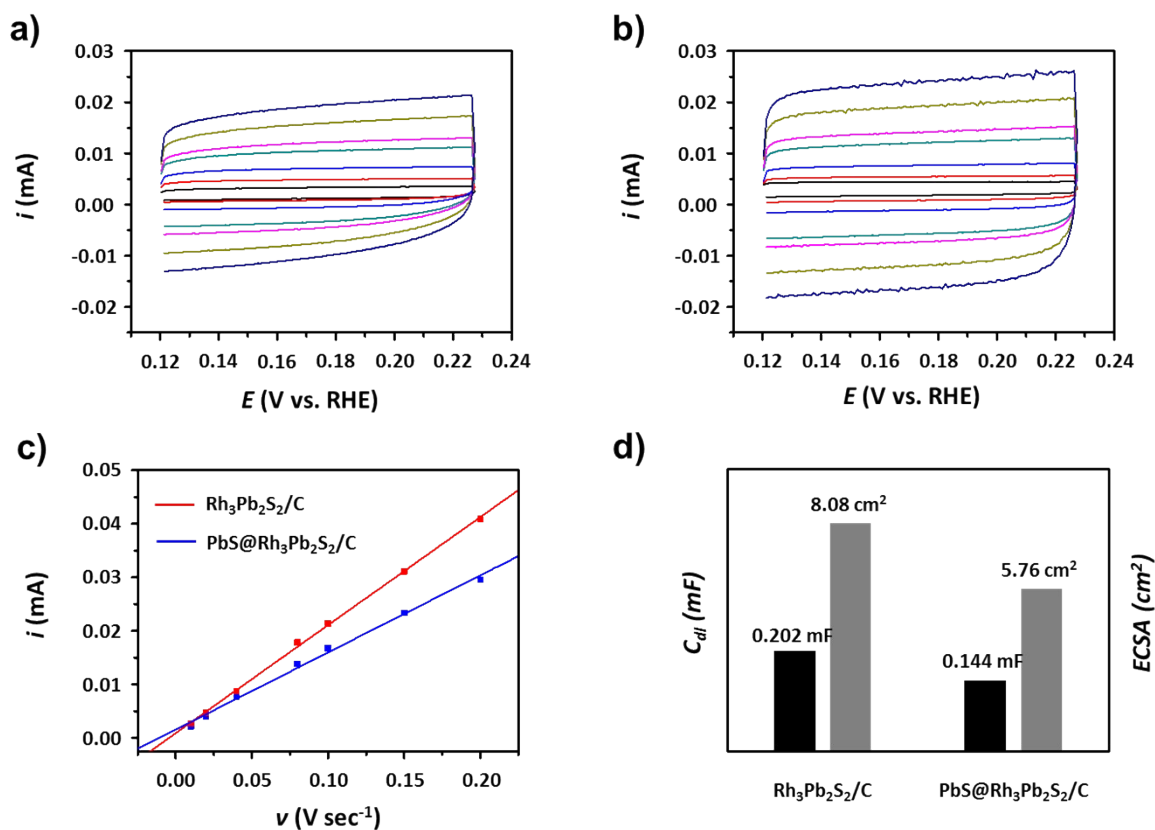


Fig. S9 The results of double-layer capacitance (C_{dl}) measurements for comparison ECSAs for PbS@Rh₃Pb₂S₂ and Rh₃Pb₂S₂ nanocages. (a) and (b) are cyclic voltammograms of PbS@Rh₃Pb₂S₂/C, and Rh₃Pb₂S₂/C, respectively, in a non-Faradaic region. The scan rates (ν) are as followed: 0.01 (black line), 0.02 (red line), 0.04 (blue line), 0.08 (cyan line), 0.1 (magenta line), 0.15 (dark yellow line), and 0.2 V sec⁻¹ (navy line). (c) A plot of currents (i) vs. scan rate (ν): the slopes (C_{dl}) are 0.202 and 0.144, which correspond to Rh₃Pb₂S₂/C (red line) and PbS@Rh₃Pb₂S₂/C (blue line), respectively. (d) A bar graph for comparison of C_{dl} and ECSAs between Rh₃Pb₂S₂/C and PbS@Rh₃Pb₂S₂/C.

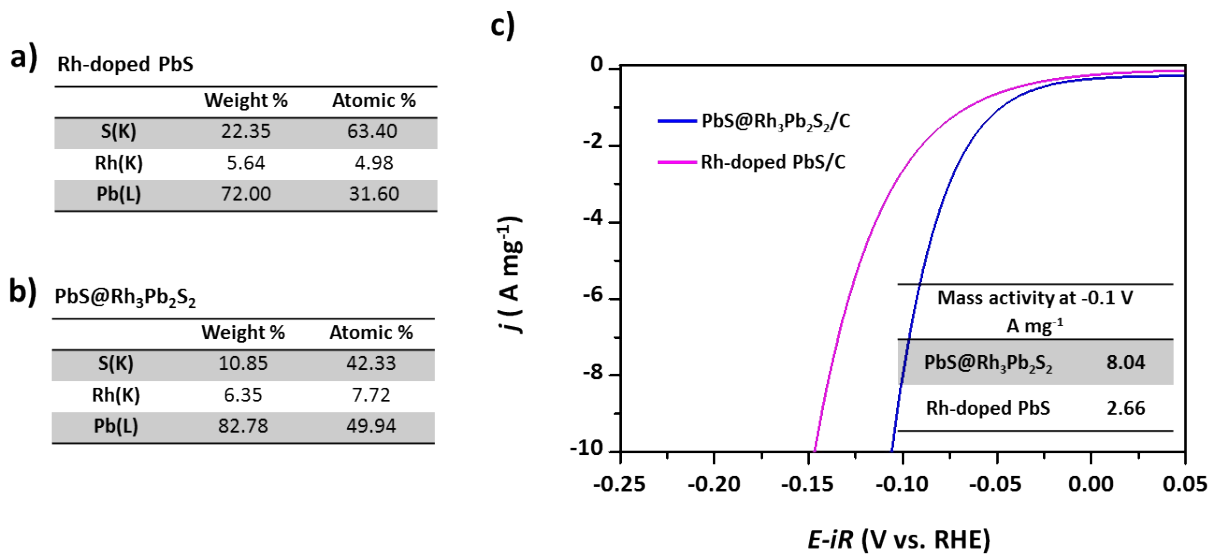


Fig. S10 EDS (energy dispersive spectroscopy) results of (a) Rh-doped PbS and (b) PbS@Rh₃Pb₂S₂ indicates their weight % and atomic % of each element. (c) The polarizability graph for mass activity processed based on their EDS data are displayed.

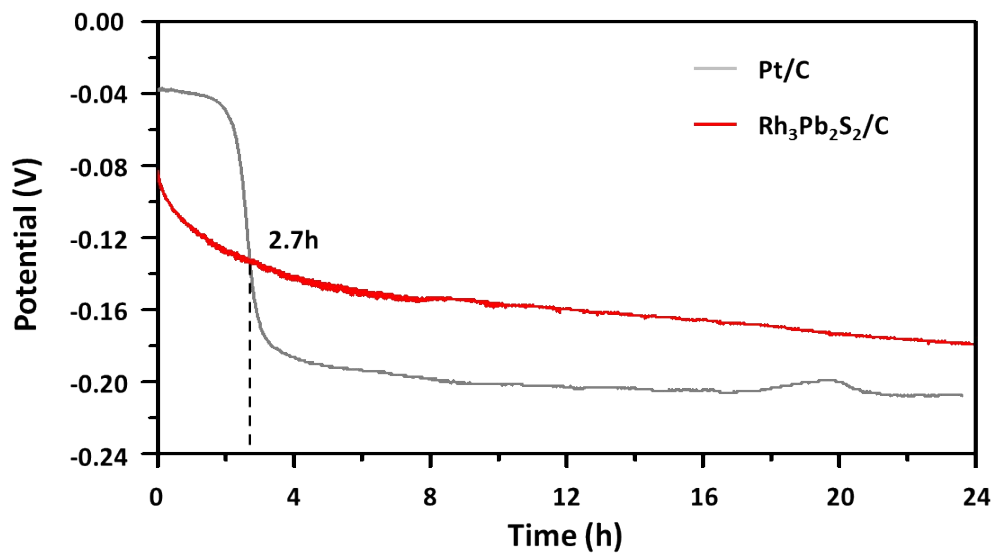


Fig. S11 Comparison of HER activities in order to maintain constant current density (-10 mA cm^{-2}) by chronopotentiometry (V-t curve) for Pt/C and Rh₃Pb₂S₂/C.

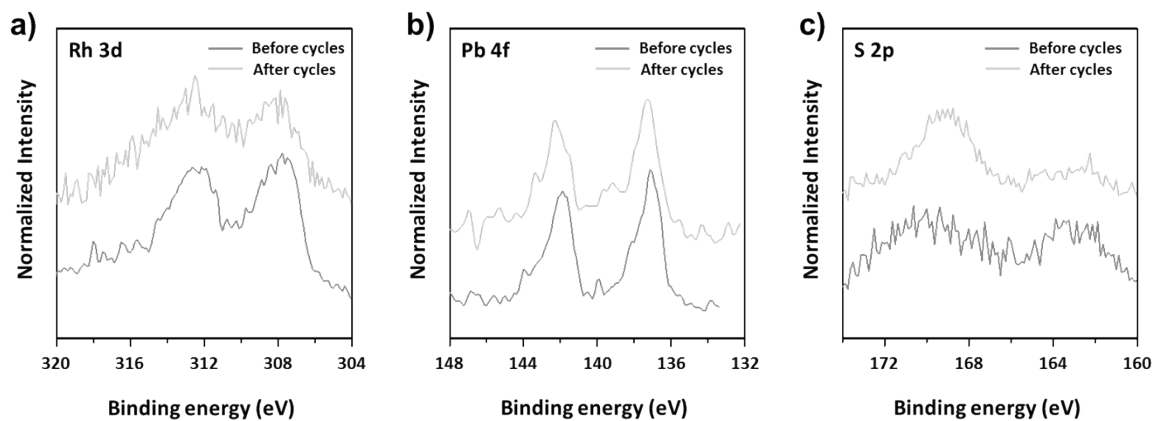


Fig. S12 X-ray photoelectron spectroscopy (XPS) spectra of $\text{Rh}_3\text{Pb}_2\text{S}_2/\text{C}$ before and after 10,000 (10k) catalytic cycling test. (a), (b), and (c) correspond to Rh 3d, Pb 4f, and S 2p peaks, respectively.

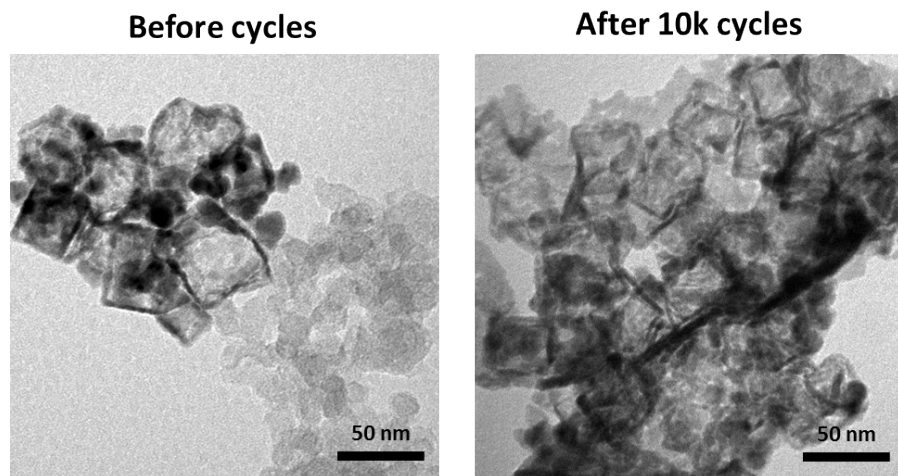


Fig. S13 TEM images of $\text{Rh}_3\text{Pb}_2\text{S}_2/\text{C}$ before and after 10,000 (10k) catalytic cycling test.

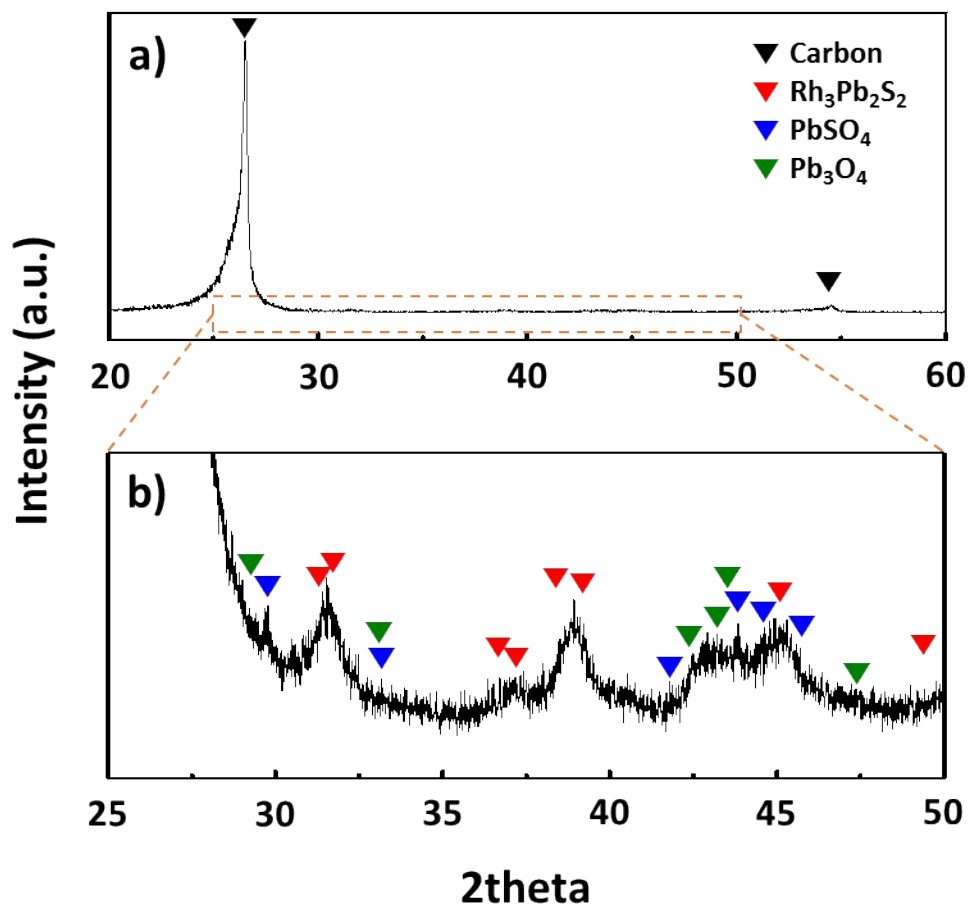


Fig. S14 XRD patterns after 10k durability test. (a) XRD patterns of carbon paper supported Rh₃Pb₂S₂ catalyst. (b) Magnification of XRD patterns of (a) from 25° to 50° (orange dotted area in (a)). JCPDS card no. 01-082-9929 for carbon (black), JCPDS card no. 01-089-2061 for Rh₃Pb₂S₂ (red), JCPDS card no. 01-083-1720 for PbSO₄ (blue), and JCPDS card no. 01-072-7379 for Pb₃O₄ (green) are displayed. (The characteristic peaks near Rh₃Pb₂S₂ patterns were indicated.)

Table S1. Contents ratio of Rh₃Pb₂S₂/C and PbS@Rh₃Pb₂S₂/C catalysts determined by ICP-AES analysis.

Sample	Weight Percent (%)			Atomic Percent (%)		
	Rh	Pb	S	Rh	Pb	S
Rh₃Pb₂S₂/C	10.7	6.6	3.2	44.1	13.5	42.4
PbS@Rh₃Pb₂S₂/C	3.9	14.4	2.4	20.7	38.2	41.0

Table S2. HER activity comparison table showing the catalyst loading, overpotential and Tafel slope.

Catalyst	Loading ($\mu\text{g cm}^{-2}$)	Overpotential (η) at 10 mA cm^{-2} (mV vs. RHE)	Tafel slope (mV dec^{-1})	Ref.
Rh₃Pb₂S₂/C	28	87.3	45.6	This work
After 10k CV cycles	28	107.6	49	This work
NiCo₂S₄ NW/NF	-	210 ^{a)}	58.9 ^{a)}	4
Zn_{0.76}Co_{0.24}S/CoS on Ti mesh	1.0 mg cm^{-2}	238 ^{a)} at 20 mA cm^{-2}	164 ^{a)}	5
Rh₂S₃-ThickHNP/C	153	122	44	6
α-INS (Iron Nickel Sulphide)	254	105	40	7
(Fe_{0.48}Co_{0.52})S₂	-	196	47.5	8
CoS₂	-	192	52	8
NiS₂	-	230 at 1 mA cm^{-2}	48.8	8
Fe_{0.9}Co_{0.1}S₂/CNT	400	160	46	9
Fe_{0.95}Co_{0.05}S₂/CNT	400	~175	~46	9
NiCo₂S₄ NA/CC	4 mg cm^{-2}	263 at 50 mA cm^{-2} ^{a)}	141 ^{a)}	10
Cu₇S₄@MoS₂	280	133	48	11
MoS₂/rGO	280	~150	41	12
ET&IE MoS₂	280	149	49	13
MoS_x/NCNT	-	110	40	14
1T-WS₂ Nanosheets	6.5	236	55	15
Metallic WS₂ Nanosheets	1 mg cm^{-2}	142	70	16
WS₂ Nanoflakes	350	100	48	17
Li-MoS₂/CF	~ 3.4 mg cm^{-2}	118	62	18
WS₂ Nanoribbons	-	225	68	19
Ni_{2.3%}CoS₂/CC	0.97 mg cm^{-2}	231 at 100 mA cm^{-2} ^{a)}	106 ^{a)}	20
MoS₃	-	~159	40	21

^{a)} Alkaline condition

- Not available to identify

~ Estimated values

◆ REFERENCES

- (1) Y. Liang, Y. Li, H. Wang, J. Zhou, J. Wang, T. Regier, H. Dai, *Nat. Mater.*, 2011, **10**, 780-786.
- (2) C. C. L. McCrory, S. Jung, J. C. Peters, T. F. Jaramillo, *J. Am. Chem. Soc.*, 2013, **135**, 16977-16987.
- (3) M. Łukaszewski, M. Soszko, A. Czerwiński, *Int. J. Electro-chem. Sci.*, 2016, **11**, 4442-4469.
- (4) A. Sivanantham, P. Ganesan, S. Shanmugam, *Adv. Funct. Mater.*, 2016, **26**, 4661-4672.
- (5) Y. Liang, Q. Liu, Y. Luo, X. Sun, Y. He, A. M. Asiri, *Electrochim. Acta*, 2016, **190**, 360-364.
- (6) D. Yoon, B. Seo, J. Lee, K. S. Nam, B. Kim, S. Park, H. Baik, S. H. Joo, K. Lee, *Energy Environ. Sci.*, 2016, **9**, 850-856.
- (7) X. Long, G. Li, Z. Wang, H. Zhu, T. Zhang, S. Xiao, W. Guo, S. Yang, *J. Am. Chem. Soc.*, 2015, **137**, 11900-11903.
- (8) M. S. Faber, M. A. Lukowski, Q. Ding, N. S. Kaiser, S. Jin, *J. Phys. Chem. C*, 2014, **118**, 21347-21356.
- (9) D. Y. Wang, M. Gong, H. L. Chou, C. J. Pan, H. A. Chen, Y. Wu, M. C. Lin, M. Guan, J. Yang, C. W. Chen, Y. L. Wang, B. J. Hwang, C. C. Chen, H. Dai, *J. Am. Chem. Soc.*, 2015, **137**, 1587-1592.
- (10) D. Liu, Q. Lu, Y. Luo, X. Sun, A. M. Asiri, *Nanoscale*, 2015, **7**, 15122-15126.
- (11) J. Xu, J. Cui, C. Guo, Z. Zhao, R. Jiang, S. Xu, Z. Zhuang, Y. Huang, L. Wang, Y. Li, *Angew. Chem. Int. Ed.*, 2016, **55**, 6502-6505.
- (12) Y. Li, H. Wang, L. Xie, Y. Liang, G. Hong, H. Dai, *J. Am. Chem. Soc.*, 2011, **133**, 7296-7299.
- (13) M.-R. Gao, M. K. Y. Chan, Y. Sun, *Nat. Commun.*, 2015, **6**, 7493.
- (14) D. J. Li, U. N. Maiti, J. Lim, D. S. Choi, W. J. Lee, Y. Oh, G. Y. Lee, S. O. Kim, *Nano Lett.* 2014, **14**, 1228-1233.
- (15) D. Voiry, H. Yamaguchi, J. Li, R. Silva, D. C. B. Alves, T. Fujita, M. Chen, T. Asefa, V. B. Shenoy, G. Eda, M. Chhowalla, *Nat. Mater.*, 2013, **12**, 850-855.
- (16) M. A. Lukowski, A. S. Daniel, C. R. English, F. Meng, A. Forticaux, R. J. Hamers, S. Jin, *Energy Environ. Sci.*, 2014, **7**, 2608-2613.
- (17) L. Cheng, W. Huang, Q. Gong, C. Liu, Z. Liu, Y. Li, H. Dai, *Angew. Chem. Int. Ed.*, 2014, **53**, 7860-7863.
- (18) H. Wang, Z. Lu, D. Kong, J. Sun, T. M. Hymel, Y. Cui, *ACS Nano*, 2014, **8**, 4940-4947.
- (19) J. Lin, Z. Peng, G. Wang, D. Zakhidov, E. Larios, M. J. Yacaman, J. M. Tour, *Adv. Energ. Mater.*, 2014, **4**, 1301875.
- (20) W. Fang, D. Liu, Q. Lu, X. Sun, A. M. Asiri, *Electrochem. Commun.*, 2016, **63**, 60-64.
- (21) Y. Li, Y. Yu, Y. Huang, R. A. Nielsen, W. A. Goddard, Y. Li, L. Cao, *ACS Catal.*, 2015, **5**, 448-455.